Is there a hot spot of sea level rise acceleration along the mid-Atlantic United States? A Gaussian process decomposition of tide gauge records

Robert E. Kopp[1]

Recent research has suggested faster-than-global acceleration of sea level rise along the northeastern coast of the United States. To test this claim, I construct a Gaussian process model of tide gauge records, decomposing the tide gauge data into a smooth, long-term trend and red noise-type short-term variability (due to short-term ocean dynamics). This approach accommodates data gaps and allows decomposition of signals into local, regional, and global components. While tide gauge records do indicate a current faster-than-global increase in the rate of sea level rise in the mid-Atlantic region, this regional acceleration could reflect either the start of a long-term trend or short-term ocean dynamics. Current tide gauge data are insufficient to discriminate between these alternatives, and they will continue to be so for about two decades.

1. Introduction

Several recent papers report an increase in the rate of sea level rise (i.e., a sea level rise acceleration) along the mid-Atlantic coast of the United States that is greater than the global average [*Sallenger et al.*, 2012; *Boon*, 2012; *Ezer et al.*, 2013]. A plausible physical mechanism for producing such an acceleration exists: a slowing Gulf Stream should reduce the dynamic sea level gradient across the North Atlantic, causing a sea level decline in the central north Atlantic and a corresponding sea level rise in the northwestern north Atlantic. A secular sea level rise associated with this mechanism is one of the few points of agreement in global climate model projections of regional sea level change [*Yin et al.*, 2009]. *Ezer et al.* [2013] suggested that changes in the Gulf Stream, reflected in the altimetry-observed alitudinal gradient across the Gulf Stream, are indeed correlated with a pronounced sea level rise in the eastern U.S. tide gauges since 2007. However, satellite altimetry of sea surface height dates back only a couple decades, so they were unable to investigate the relationship between the Gulf Stream gradient and tide gauges before 1993.

Regional and local sea level differ from mean global sea level (GSL) due to several factors. Glacial isostatic adjustment (GIA), which is driven by the viscous response of the mantle to the changes in ice mass loads since the Last Glacial Maximum, is causing the collapse of the proglacial forebulge in the mid-Atlantic region and the uplift of the Hudson Bay area. Land subsidence in the mid-Atlantic region leads to a sea level rise, partially mitigated by the geoid shift caused by the emplacement of mass underneath Hudson Bay [*Peltier*, 2004]. GIA is a slow, long-term process; rates of GIA-driven sea level change are close to linear on the scale of the observational record. East of the Fall Line, which passes close to New York City, Baltimore, and Washington, bedrock is overlain by the Mesozoic and Cenozoic sediments of the Coastal Plain, which can subside due to natural compaction and therefore experience a faster long-term rate of sea level rise. In the southern region of the Chesapeake Bay, high rates of subsidence may also be attributable to brecciation by the late Eocene Chesapeake Bay impact [*Poag*, 1997].

On shorter timescales, regional sea level anomalies can arise from land ice melt and ocean dynamics [e.g., *Kopp et al.*, 2010]. Melting land ice leads to a slower or negative sea level rise near the meltwater source, and an enhanced sea level rise far from the source [*Farrell and Clark*, 1976; *Mitrovica et al.*, 2001]. Greenland melt will thus produce less-than-global sea level rise on the Eastern seaboard of the United States, while Antarctic melt will produce greater-than-global sea level rise [*Mitrovica et al.*, 2001, 2009]. Regional anomalies also arise from changes in ocean dynamic factors such as Gulf Stream strength, as previously noted; these factors can undergo both strong interannual variability and lower frequency variations. Local sea level anomalies can also arise from direct anthropogenic effects such as groundwater withdrawal and dredging.

Here we develop a new spatio-temporal statistical method for analyzing tide gauge data, with the goal of partially disaggregating the sources of sea level rise. The method, based upon Gaussian process regression [*Rasmussen and Williams*, 2006] (alternatively known as spatio-temporal krieging) is well-suited for investigating possible regional accelerations for several reasons. First, it is fully probabilistic, so measurement and inferential uncertainties are propagated through the entire analysis. Second, it models sea level as a spatio-temporal field, naturally identifying regions with coherent sea level signals and appropriately sharing information among neighboring sites in the calculation of posterior sea level estimates. Third, being Bayesian in derivation (though empirical, rather than fully, Bayesian in implementation), it copes naturally with the missing data that characterize tide gauge records. Fourth, it is non-parametric, and so does not force a functional form on the interpretation of the tide gauge records (in contrast to the approaches of *Sallenger et al.* [2012] and *Boon* [2012]). It does, however, employ a parametric estimate of the prior covariance of sea level; this parameterized covariance allows easy separation of global, regional, and local signals, and of linear trends, smooth but non-linear variability, and red noise variability.

Below, I demonstrate this method through application to tide gauge records from the eastern coast of North America and employ it to assess claims about a regional "hot spot" of sea level rise acceleration.

2. Methods

2.1. Statistical framework

Sea level is a spatio-temporal field, which we model as a mean zero Gaussian process

$$f(\mathbf{x}, t) \sim \mathcal{GP}(\mathbf{0}, \mathbf{\Sigma}) \quad (1)$$

[1]Department of Earth & Planetary Sciences and Rutgers Energy Institute, Rutgers University, Piscataway, NJ 08854, USA. (robert-dot-kopp-at-rutgers-dot-edu)

which we observe, through tide gauges, with independent but potentially heteroscedastic noise

$$s(\mathbf{x},t) = f(\mathbf{x},t) + \epsilon(\mathbf{x},t). \quad (2)$$

The covariance $\mathbf{\Sigma}$ is the sum of nine terms, representing all combinations of three different temporal covariance functions and three different spatial covariance functions. For each term, the spatial and temporal covariances are separable, though as the length scales of each spatial-temporal covariance pair are different, they are not collectively so. The three temporal covariances have the forms of dot product (denoted by superscript ^{l}), rational quadratic (^{q}), and exponential covariances (^{n}). The dot product terms correspond to linear trends; the latter two terms are stationary, and represent respectively smooth variations around the trend and high-frequency, red noise-type variability. The three spatial covariances represent globally uniform ($_g$), regionally-specific ($_r$), and site-specific components ($_l$).

$$\mathbf{\Sigma} = \mathbf{\Sigma}^l + \mathbf{\Sigma}^q + \mathbf{\Sigma}^n \quad (3)$$

$$\mathbf{\Sigma}^l_{i,j} = (t_i t_j) \times \big[\sigma_g^{l2} + \sigma_r^{l2} C(\Delta\mathbf{x}_{i,j}, \frac{5}{2}) + \sigma_n^{l2}\delta_{i,j} \cdot I(i \in \mathrm{CP}, j \in \mathrm{CP})\big] \quad (4)$$

$$\mathbf{\Sigma}^q_{i,j} = \Big(1 + \frac{\Delta t_{i,j}^2}{2\alpha\tau^{q2}}\Big)^{-\alpha} \times \big[\sigma_g^{q2} + \sigma_r^{q2} C(\Delta\mathbf{x}_{i,j}, \frac{5}{2}) + \sigma_n^{q2}\delta_{i,j}\big] \quad (5)$$

$$\mathbf{\Sigma}^n_{i,j} = \exp(\frac{-\Delta t_{i,j}}{\tau^n}) \times \big[\sigma_g^{n2} + \sigma_r^{n2} C(\Delta\mathbf{x}_{i,j}, \frac{5}{2}) + \sigma_n^{n2}\delta_{i,j}\big] \quad (6)$$

$$C(r,v,\gamma) = \frac{2^{1-v}}{\Gamma(v)}\Big(\frac{\sqrt{2v}r}{\gamma}\Big) K_v\Big(\frac{\sqrt{2v}r}{\gamma}\Big) \quad (7)$$

where $C(r,v,\gamma)$ is a Matérn covariance function of order γ, $\Delta x_{i,j}$ is the angular distance between points i and j, $\Delta t_{i,j}$ is the temporal distance $t_i - t_j$, and $\delta_{i,j}$ is the Kronecker delta function. We interpret the regional, linear term as being due to GIA. $I(i \in \mathrm{CP}, j \in \mathrm{CP})$ is an indicator function that is equal to 1 if sites i and j are both located on Coastal Plain sediments and 0 if either site is located on bedrock; that is to say, for sites on bedrock we interpret all local linear trends as reflecting the regional GIA signal.

We can condition upon observations $\mathbf{s}$ and hyperparameters θ to estimate the posterior distribution of f at points $(\mathbf{x}_*, t_*)$, which we denote as $\mathbf{f}_*$:

$$\mathbf{f}_*|\mathbf{s},\theta \sim \mathcal{N}(\mathbf{\Sigma}_{*,\mathbf{s}}(\mathbf{\Sigma}_\mathbf{s} + \mathbf{\Gamma}_\epsilon)^{-1}\mathbf{s}, \mathbf{\Sigma}_* - \mathbf{\Sigma}_{*,\mathbf{s}}(\mathbf{\Sigma}_\mathbf{s} + \mathbf{\Gamma}_\epsilon)^{-1}\mathbf{\Sigma}_{*,\mathbf{s}}{}^\top) \quad (8)$$

where $\mathbf{\Gamma}_\epsilon$ is the diagonal matrix of observation errors and $\mathbf{\Sigma}_\mathbf{s}$, $\mathbf{\Sigma}_*$, and $\mathbf{\Sigma}_{*,\mathbf{s}}$ represent respectively the covariance matrix for the points at which the observations $\mathbf{s}$ are taken, the covariance matrix for the desired points, and the covariance matrix between the desired points and the observed points. To isolate certain components of sea level in estimating $\mathbf{f}_*$ (for example, to estimate only the component corresponding to the regional rational quadratic covariance function), we include in $\mathbf{\Sigma}_*$ and $\mathbf{\Sigma}_{*,\mathbf{s}}$ only the desired components. (See Fig. 1 for an example decomposition of the New York City (Battery) tide gauge record.) Note that this approach gives us a full posterior probability distribution, including the off-axis covariance terms. Accordingly, we can, through sampling, assess extreme value questions; for example, we can compare how a current rate of change compares to all rates of change during the last century.

For the remainder of the paper, we use the term "sea level anomaly" to refer to the regional and local components of sea level (σ_r and σ_n terms), "regional sea level anomaly" to refer to the regional components of sea level (σ_r terms), "smooth sea level anomaly" to refer to those components reflected in the temporally linear ($\mathbf{\Sigma}^l$) and rational quadratic ($\mathbf{\Sigma}^q$) terms, and "non-linear sea level anomaly" to refer to these components reflected in the temporally rational quadratic and red noise-type terms ($\mathbf{\Sigma}^n$). A regional acceleration in sea level rise that is faster than the global average would accordingly be reflected by an accelerating rise in the smooth, regional sea level anomaly.

2.2. Hyperparameters

We denote the vector of spatial hyperparameters as $\theta_x = \{\sigma_g^l, \sigma_r^l, \sigma_n^l, \gamma^l, \sigma_g^q, \sigma_r^q, \sigma_n^q, \gamma^q, \sigma_g^n, \sigma_r^n, \sigma_n^n, \gamma^n\}$ and the vector of temporal hyperparameters as $\theta_t = \{\alpha, \tau^q, \tau^n\}$. Rather than specifying priors over all of the hyperparameters, which would be the fully Bayesian approach, for computational efficiency we adopt an empirical Bayesian approach, estimating the values of the hyperparameters that maximizes the likelihood of the observations. For computational efficiency and interpretive ease, we adopt a staged approach. First, we optimize θ_t individually for each tide gauge and then fix θ_t at the value of the median across tide gauges. To ensure that the selected hyperparameters separate red noise-type variability and smoother variations as intended, we bound $\tau^q \leq 1000$ y and $\alpha \geq 0.05$. Next, we fix the globally constant amplitudes $\{\sigma_g^l, \sigma_g^q, \sigma_g^n\}$ at the values that maximize the likelihood of the *Church and White* [2011] estimate of GSL. Third, we find the values of σ_r^l and γ^l that maximizes the likelihood of a Gaussian process, Matérn covariance fit to the GIA rates of *Peltier* [2004]. Finally, we find the maximum likelihood values of the remaining hyperparameters, using the median of the maximum likelihood parameters calculated with 20 data subsets. Each data subset consists of four mid-Atlantic tide gauges (Philadelphia, New York, Sandy Hook and Atlantic City) and twenty-five randomly selected 20-year blocks from other tide gauges. We employ high subset coverage in the mid-Atlantic because of the high spatial density of tide gauges in this region. Optimized hyperparameters are shown in Table 1.

2.3. Data

We analyze estimates of mean annual sea level from the forty-seven eastern North America tide gauges archived by the Permanent Service for Mean Sea Level (http://www.psmsl.org/) with a record length exceeding thirty years. The gauges stretch from Daytona Beach, Florida, to St. John's, Newfoundland (Fig. S1). We indirectly incorporate data from other sites through the use of the *Church and White* [2011] estimate of GSL. Tide gauge observation errors are assumed to be ± 6 mm (2σ).

3. Decomposition of tide gauge signals

3.1. Long-term trends

The linear trends projected at each site differ significantly from those projected using the ICE-5G VM2-90 glacio-isostatic adjustment model of *Peltier* [2004] (Figs. 2, S2). The discrepancy is particularly severe in Virginia, where the GIA projections lay outside the 95% confidence interval of the trend estimate. However, nowhere except between Massachusetts and Pennsylvania and in South Carolina, north Florida, and parts of eastern maritime Canada do the ICE-5G projections fall within the 67% confidence interval of our inferred regional linear trends. Where data exists, our results are generally in agreement (within uncertainty) with

the long-term rates of sea level rise estimated from multiple millennia of geological sea level proxies by *Engelhart et al.* [2009]. The notable exception to this agreement is on the Eastern Shore of the Chesapeake Bay, in Virginia, where the high linear trend seen in the tide gauge record is not matched in the geological record.

The discrepancy between ICE-5G estimates and the observed long-term trends suggests either considerable error in the VM2-90 solid Earth parameters or the ICE-5G ice sheet history, or a major role for additional factors such as sediment compaction in the regions of discrepancy. Sediment compaction may well be quite significant; the Virginia sites lay largely on Coastal Plain sediments in which compaction could well play an important role. In addition to the Virginia sites, high linear rates of sea level rise relative to the projected regional trend are observed on the Coastal Plain of New Jersey at Sandy Hook and Atlantic City. The geographic spread of the high rate of sea level rise on the coastal plain throughout the mid-Atlantic region, not just in the vicinity of the Chesapeake Impact structure, suggests a dominant role for sediment compaction not related to the impact. Nevertheless, we do note considerable local variability among the four sites in the southern Chesapeake vicinity of the impact structure, with long term rates ranging from 1.7 ± 0.8 (2σ) mm/y at Kipotopeke to 2.6 ± 0.6 mm/y at Sewells Point (Fig. S2).

3.2. Non-linear component of regional sea level

Fig. 3 shows the non-linear sea level anomaly. In Fig. 3d, four regionally coherent features stand out: significant rates of sea level anomaly rise along the entire seaboard in the 1930s and 1940s; significant rates of sea level anomaly fall in the mid-Atlantic region in the 1970s, followed by slightly delayed fall to the north; and current significant rates of sea level anomaly rise in the mid-Atlantic and significant rates of sea level anomaly fall in the southeastern U.S.

The sea level anomaly rise in the 1930s and 1940s is contemporaneous with high rates of GSL rise, as can also be seen by examining the New York City tide gauge record (Fig. 1). The behavior of the Greenland ice sheet during this period is currently the subject of considerable disagreement [*Gregory et al.*, 2013], with some modelers suggesting that the warm Northern Hemisphere temperatures of the 1930s drove strong Greenland melt and others suggesting that it drove enhanced accumulation. The observed pattern of greater-than-global sea level rise off of North America during this interval is consistent with that expected from West Antarctic Ice Sheet melt and the opposite of what would be expected from the static sea level fingerprint of Greenland melt [*Mitrovica et al.*, 2001, 2009]. However, the effects on the Gulf Stream of Greenland melt might be expected to operate in the opposite direction [*Kopp et al.*, 2010]; it is therefore not possible from regional data alone to infer the role of Greenland in the 1930s and 1940s. A global analysis along the lines proposed by *Hay et al.* [2013] might succeed in this regard.

In the mid-Atlantic region, the sea level anomaly fall in the 1970s and subsequent sea level anomaly rise in the 1990s and 2000s give rise to the "hot spot" of sea level rise acceleration noted by other authors. We address the robustness and uniqueness of this feature below.

4. A sea level rise hot spot?

A weakening or migrating Gulf Stream will give rise to a reduction in the negative sea surface height gradient that runs north along the eastern North American coast [*Yin et al.*, 2009]. In tide gauge records that use as a reference datum local sea level in a common year, this will appear as an increasing gradient between the northeast and the southeast. To evaluate the mid-Atlantic "hot spot," we therefore consider the difference in the non-linear regional sea level anomaly between New York City and Charleston (Fig. 4). The analysis removes the signals associated with global sea level change, with long-term linear changes due to effects such as GIA, and with purely local effects.

Between 1990 and 2012, the smooth, non-linear regional sea level gradient between New York City and Charleston increased by 16 ± 25 mm (an average rate of 0.7 ± 1.1 mm/y); it is therefore very likely (probability $\sim 90\%$) that the gradient has increased over this time period. The mid-Atlantic hot spot as such therefore does appear to be fairly robust. Its robustness does not, however, necessarily imply that the recent increases marks the start of a secular change in the Gulf Stream; it could reflect variability within the system.

The greatest increase in the gradient over any 22-year period starting no earlier than 1900 and ending no later than 1990 was 25 mm (95% range of 3–82 mm) (0.8 mm/y, range of 0.1–3.7 mm/y). It is likely (probability $\sim 72\%$) that the rate of the 1990-2012 rise was exceeded at some point during the rest of the twentieth century.

The magnitude of the gradient, referenced to the expected value in 1900 as a common datum, is currently 6 ± 38 mm, about 11 ± 26 mm below the maximum value attained between 1900 and 1990. The current magnitude will need to increase by about 16 mm before it can be identified as likely (probability $>\sim 67\%$) unprecedented within the twentieth century and by about 28 mm before it can be identified as very likely unprecedented. At the average rate of increase of the last 22 years, this would take about 20 and 40 years, respectively. However, it is likely (probability $\sim 80\%$) that the current rate of increase, estimated at 0.3 ± 2.2 mm/y, is less than the average over 1990-2012.

Yin et al. [2009] project that, under the A1B scenario, a weakening Atlantic Meridional Overturning Circulation will give establish a ~ 150 mm dynamic sea level gradient between New York and Miami during the century between 1980-2000 and 2080-2100. The gradient between New York and Charleston will be similar. For such a gradient to be attained, another ~ 130 mm increase must occur over the next ~ 80 years, on top of the ~ 16 mm that has occurred since 1990. Achieving the gradient increase will require an acceleration in the rate of increase of ~ 0.04 mm/y^2. Comparing the mean rates of change over 1968-1990 to that over 1990-2012, we find an average acceleration of 0.05 ± 0.08 mm/y^2, which would likely be sufficient if sustained. It is about as likely as not (probability $\sim 43\%$) that this acceleration was unprecedented in the rest of the twentieth century. If this acceleration were to continue for about two decades, the average rate of change would attain a likely unprecedented value of about 1.7 mm/y.

While the current analysis is consistent with previous work identifying a recent shift to faster-than-global sea level rise in the mid-Atlantic region, neither the magnitude of the phenomenon, nor its rate of change, nor the acceleration of its rate of change appear to be beyond the bounds of twentieth-century variability. It is therefore premature to evaluate *Sallenger et al.* [2012]'s hypothesis that the current regionally high rates of sea level rise along the U.S. east coast represent the start of a long-term reorganization of the Gulf Stream, and it will take about two decades of additional observations before the sea level effects of such a reorganization can be identified in tide gauge records.

Acknowledgments. This work was supported by NSF grant ARC-1203415 and inspired by the Sea Level Rise Expert Group of the Maryland Climate Change Commission. I thank K. Miller, B. Horton, A. Kemp and V. Pavlovic for helpful discussion.

Table 1. Optimized hyperparameters

σ_g^l	1.7	global linear amplitude (mm/y)
σ_g^q	36.1	global rational quadratic amplitude (mm)
σ_g^n	0	global red noise amplitude (mm)
σ_r^l	1.6	regional linear amplitude (mm/y)
σ_r^q	29.7	regional rational quadratic amplitude (mm)
σ_r^n	28.8	regional red noise amplitude (mm)
σ_l^l	0.5	local linear amplitude (mm/y)
σ_l^q	28.9	local rational quadratic amplitude (mm)
σ_l^n	11.9	local red noise amplitude (mm)
τ^q	1,000	rational quadratic timescale
α	.05	rational quadratic smoothness
τ^n	1.0	red noise timescale (y)
γ^l	6.4	regional linear length scale (degrees)
γ^r	4.2	regional rational quadratic length scale (degrees)
γ^n	7.6	regional red noise length scale (degrees)

References

Boon, J. D. (2012), Evidence of Sea Level Acceleration at US and Canadian Tide Stations, Atlantic Coast, North America, *J. Coastal Res.*, *28*(6), 1437–1445, doi:10.2112/JCOASTRES-D-12-00102.1.

Church, J., and N. White (2011), Sea-level rise from the late 19th to the early 21st century, *Surveys in Geophysics*, *32*(4), 585–602, doi:10.1007/s10712-011-9119-1.

Engelhart, S. E., B. P. Horton, B. C. Douglas, W. R. Peltier, and T. E. Törnqvist (2009), Spatial variability of late Holocene and 20th century sea-level rise along the Atlantic coast of the United States, *Geology*, *37*(12), 1115–1118, doi:10.1130/G30360A.1.

Ezer, T., L. P. Atkinson, W. B. Corlett, and J. L. Blanco (2013), Gulf Stream's induced sea level rise and variability along the US mid-Atlantic coast, *J. Geophys. Res.*, *118*, 685–697, doi:10.1002/jgrc.20091.

Farrell, W. E., and J. A. Clark (1976), On postglacial sea level, *Geophys. J. R. Astron. Soc.*, *46*(3), 647–667, doi:10.1111/j.1365-246X.1976.tb01252.x.

Fenneman, N. M., and D. W. Johnson (1946), Physiographic divisions of the conterminous U.S. U.S. Geological Survey.

Gregory, J. M., N. J. White, J. A. Church, M. F. P. Bierkens, J. E. Box, M. R. van den Broeke, J. G. Cogley, X. Fettweis, E. Hanna, P. Huybrechts, L. F. Konikow, P. W. Leclercq, B. Marzeion, J. Oerlemans, M. E. Tamisiea, Y. Wada, L. M. Wake, and R. S. van de Wal (2013), Twentieth-century global-mean sea-level rise: is the whole greater than the sum of the parts?, *J. Climate*, doi:10.1175/JCLI-D-12-00319.1.

Hay, C. C., E. Morrow, R. E. Kopp, and J. X. Mitrovica (2013), Estimating the sources of global sea level rise with data assimilation techniques, *Proc. Natl. Acad. Sci. USA*, *110*(S1), 3692–3699, doi:10.1073/pnas.1117683109.

Kopp, R. E., J. X. Mitrovica, S. M. Griffies, J. Yin, C. C. Hay, and R. J. Stouffer (2010), The impact of Greenland melt on local sea levels: a partially coupled analysis of dynamic and static equilibrium effects in idealized water-hosing experiments, *Climatic Change*, *103*, 619–625, doi:10.1007/s10584-010-9935-1.

Mitrovica, J. X., M. E. Tamisiea, J. L. Davis, and G. A. Milne (2001), Recent mass balance of polar ice sheets inferred from patterns of global sea-level change, *Nature*, *409*(6823), 1026–1029, doi:10.1038/35059054.

Mitrovica, J. X., N. Gomez, and P. U. Clark (2009), The sea-level fingerprint of West Antarctic collapse, *Science*, *323*(5915), 753–753, doi:10.1126/science.1166510.

Peltier, W. (2004), Global glacial isostasy and the surface of the ice-age earth: The ICE-5G (VM2) model and GRACE, *Annu. Rev. Earth Planet. Sci.*, *32*, 111–149, doi:10.1146/annurev.earth.32.082503.144359.

Poag, C. W. (1997), The Chesapeake Bay bolide impact: a convulsive event in Atlantic Coastal Plain evolution, *Sed. Geol.*, *108*(1–4), 45–90, doi:10.1016/S0037-0738(96)00048-6.

Rasmussen, C., and C. Williams (2006), *Gaussian processes for machine learning*, MIT Press, Cambridge, MA.

Sallenger, A. H., K. S. Doran, and P. A. Howd (2012), Hotspot of accelerated sea-level rise on the Atlantic coast of North America, *Nat. Climate Change*, doi:10.1038/nclimate1597.

Yin, J., M. E. Schlesinger, and R. J. Stouffer (2009), Model projections of rapid sea-level rise on the northeast coast of the United States, *Nat. Geosci.*, *2*(4), 262–266, doi:10.1038/ngeo462.

Zervas, C. E. (2003), Long term changes in tidal response associated with the deepening of navigagional channels, in *Proc. 13th Bienncial Coastal Zone Conference*, Baltimore, MD.

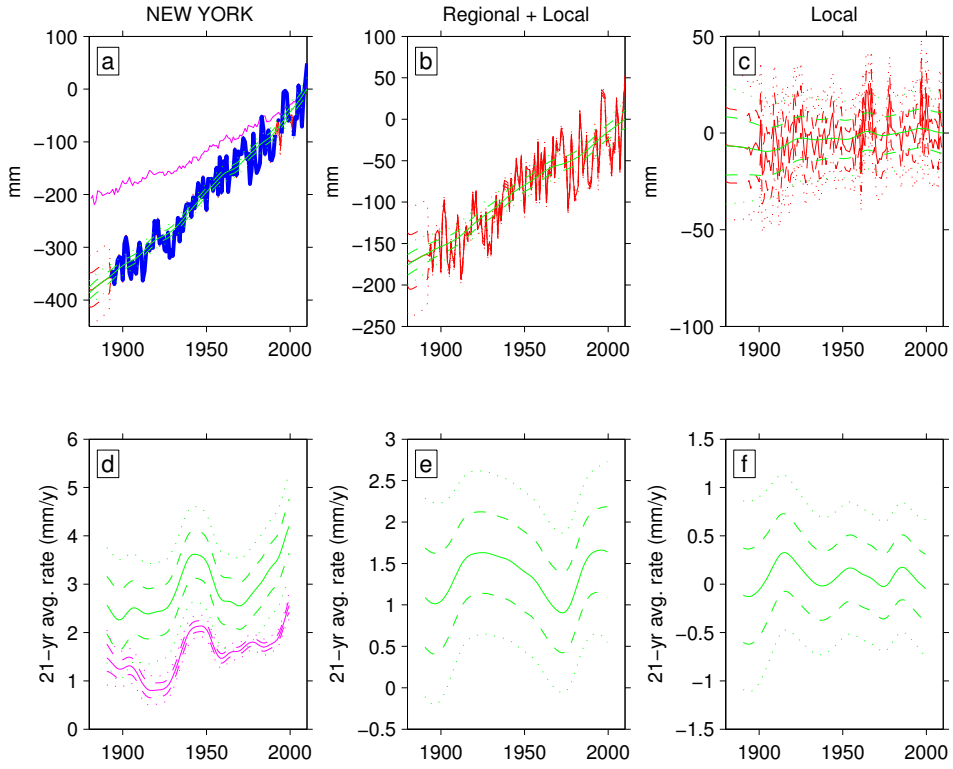

Figure 1. Example sea level decomposition. (a) Sea level at the Battery (blue), modeled underlying sea level field (red), and modeled underlying field without AR(1) component (green). Church and White estimate of GSL shown for comparison (magneta). (b) The regionally and locally varying components of the sea level field at the battery. (c) The locally varying component of the sea level field. (d-f) corresponding 21-year running mean derivatives of the green curves in (a-c). The magneta curve in (d) is the corresponding GSL rate curve. Dashed and dotted lines show 67% and 95% confidence intervals, respectively.

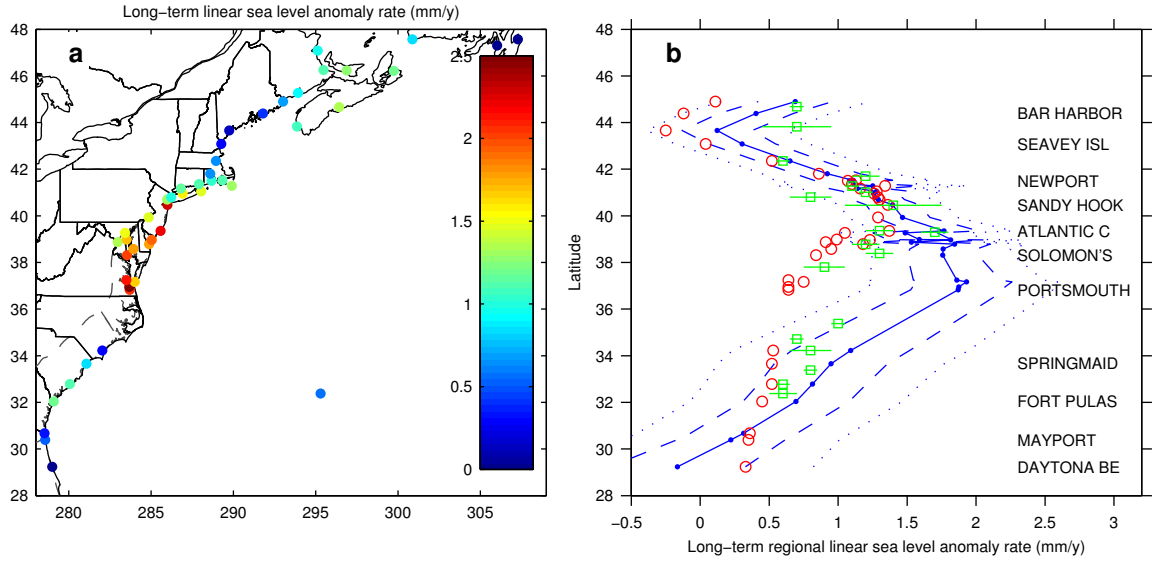

Figure 2. (a) Map of mean estimate of long-term linear sea level anomaly rate (i.e., change in sea level with respect to GSL). Dotted grey curves denotes the boundaries of the Coastal Plain provinces [*Fenneman and Johnson*, 1946]. (b) Regional linear sea level anomaly rates along the U.S. coast (blue; dashed=67% confidence interval, dotted=95% confidence interval), compared to ICE-5G projections of GIA-associated rates of sea level rise (red) [*Peltier*, 2004] and to the geological estimates of late Holocene sea level rise of *Engelhart et al.* [2009] (green; lines=1σ errors).

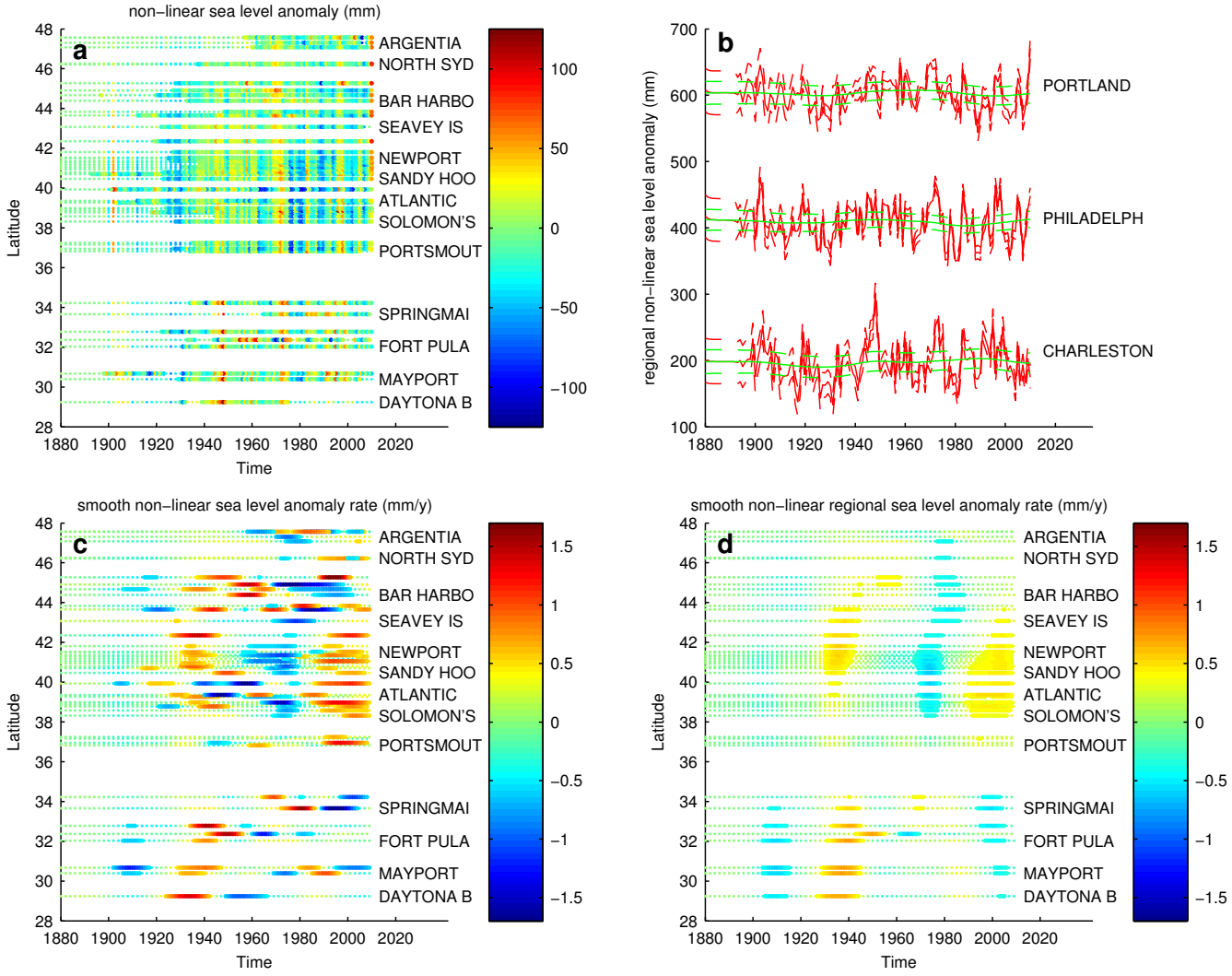

Figure 3. (a,b) Non-linear component of sea level anomaly and (c,d) smooth non-linear component of sea level anomaly rates. (b,d) show the regional component only, with (b) showing the expression and three specific localities. In (a), heavy regions indicate space-time points where the standard deviation of the non-linear sea level anomaly estimate is < 20 mm. In (b), the green curves show the smooth component. Dashed lines denote 67% confidence interval. In (c,d), heavy regions indicate space-time points where it is likely (probability $> 67\%$) that the sign of the sea level anomaly rate component is correctly identified.

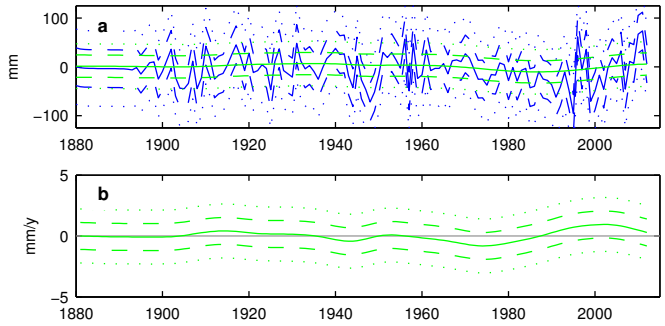

Figure 4. The difference in the regional sea level anomaly at New York City and Charleston, South Carolina. Blue curves include red-noise type variability; green curves include only the smooth component. (a) Amplitude of the anomaly gradient, (b) rate of change. Dashed (dotted) lines denote 67% (95%) confidence intervals.

Supplementary text

Optimized hyperparameters

Optimized hyperparameters are shown in Table 1. The timescale of the red noise-type variability τ^n is 1 year. The rational quadratic parameters τ^q and α are fixed at their bounds, to facilitate interpretation; unconstrained optimization would lead the rational quadratic terms to incorporate some of the short-term variability accounted for b the red noise term. The length scales of the regional linear (γ^l), rational quadratic (γ^q) and red noise (γ^n) terms are respectively 6.4, 4.2, and 7.6 degrees. No red noise term is needed for the global sea level curve ($\sigma_g^n = 0$), which can be fully accommodated within its estimation error by smooth variability around a linear trend. At a regional scale, variability around the linear trend is accounted for in roughly equal proportion by smooth variations ($\sigma_r^q = 29.7$ mm) and red noise ($\sigma_r^n = 28.8$ mm). Smooth local variations are comparable in magnitude to regional variations ($\sigma_l^q = 29.7$ mm), while local red noise is smaller ($\sigma_l^n = 11.9$ mm).

Local non-linear sea level

Examination of the non-linear local components highlights a few localities where the deviation of the non-linear components of local sea level from regional sea level are exceptionally high, as defined by the variance of the non-linear components. In particular, the five sites with at least half a century of data constituting top ten percent of variances are, in ranked order: St. John, New Brunswick; Philadelphia, Pennsylvania, Eastport, Maine; Portland, Maine; and Wilmington, North Carolina. Two of the sites are on the Gulf of Maine, and a third on the Bay of Fundy, and they are likely subject to high-amplitude, short wavelength dynamic variability. The Philadelphia tide gauge (Fig. S3) is located on the Delaware River, and the Wilmington tide gauge (Fig. S4) is located on the Cape Fear River. Both rivers have been dredged during the twentieth-century [*Zervas*, 2003]; the combination of dredging and natural riverine dynamics may account for the observed signals.

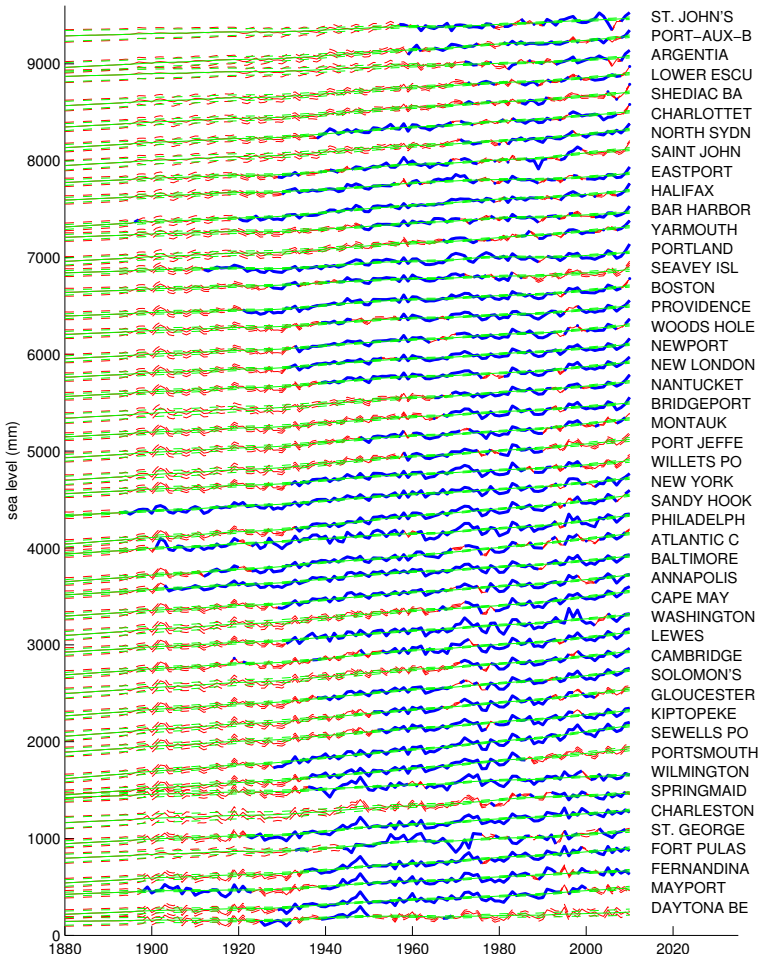

Figure S1. Tide gauge observations (blue) and the estimated underlying sea level field (red; dotted=67% confidence interval). Green curves exclude red noise-type variability. Tide gauges presented from north to south.

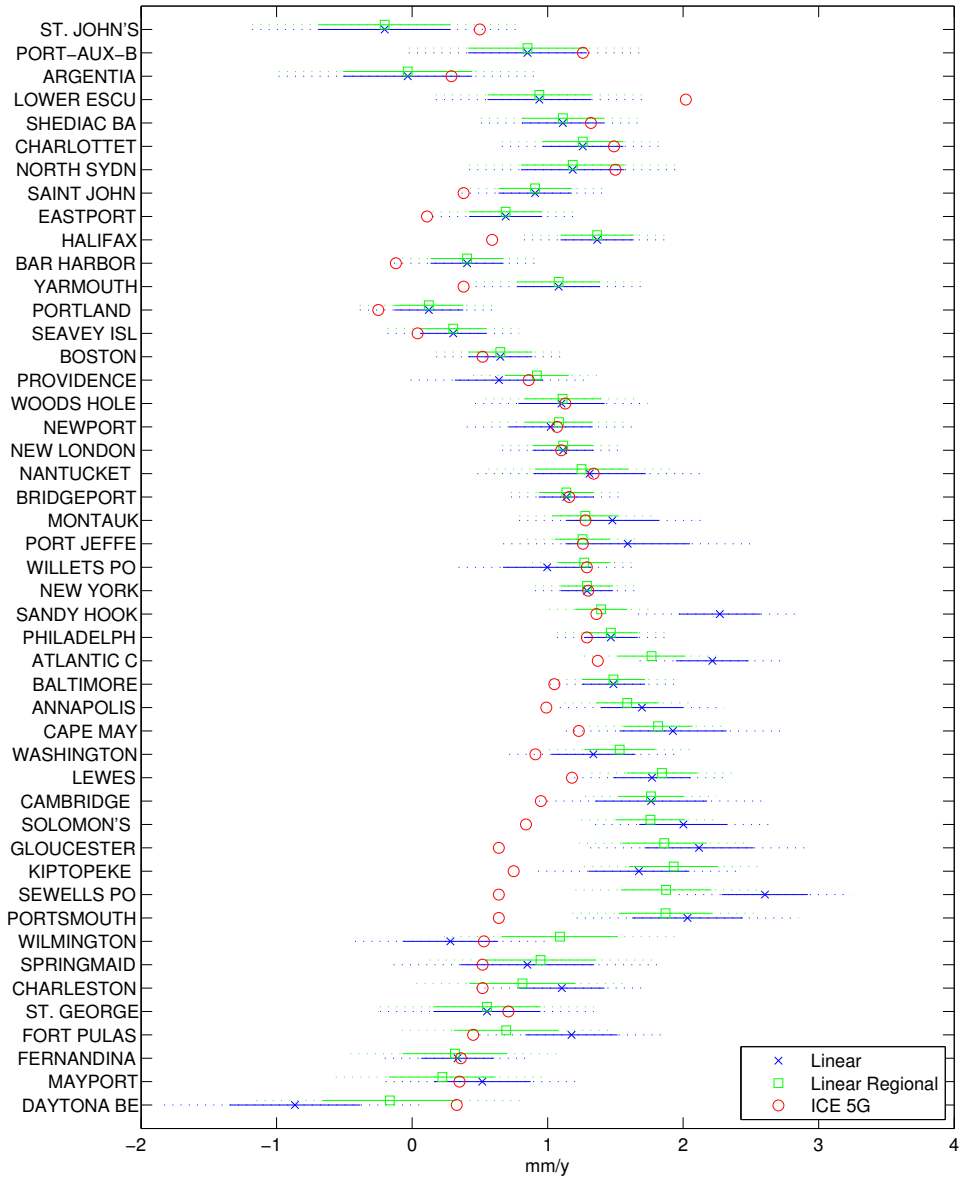

Figure S2. Estimated linear component of sea level anomaly rate (blue = regional + local signal; green = regional signal only) compared to the ICE5G VM2-90 GIA estimates.

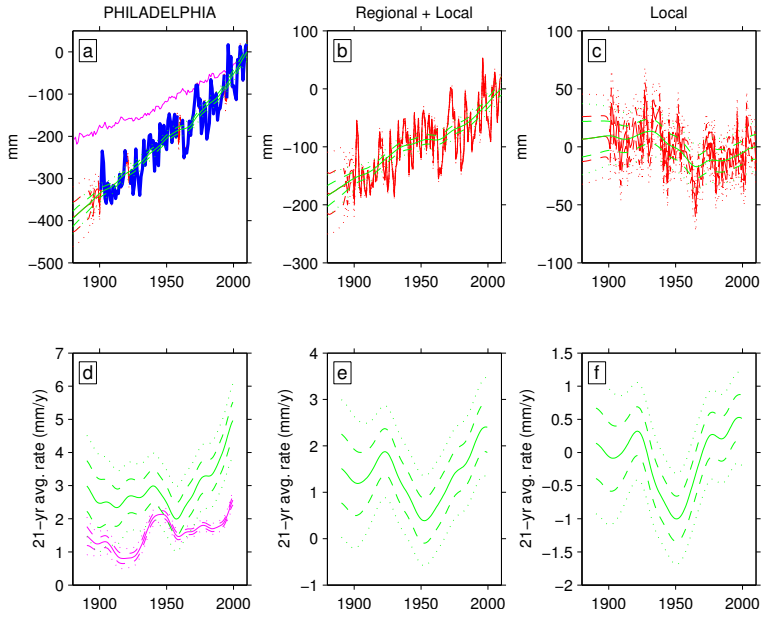

Figure S3. Sea level decomposition for the tide gauge at Philadelphia.

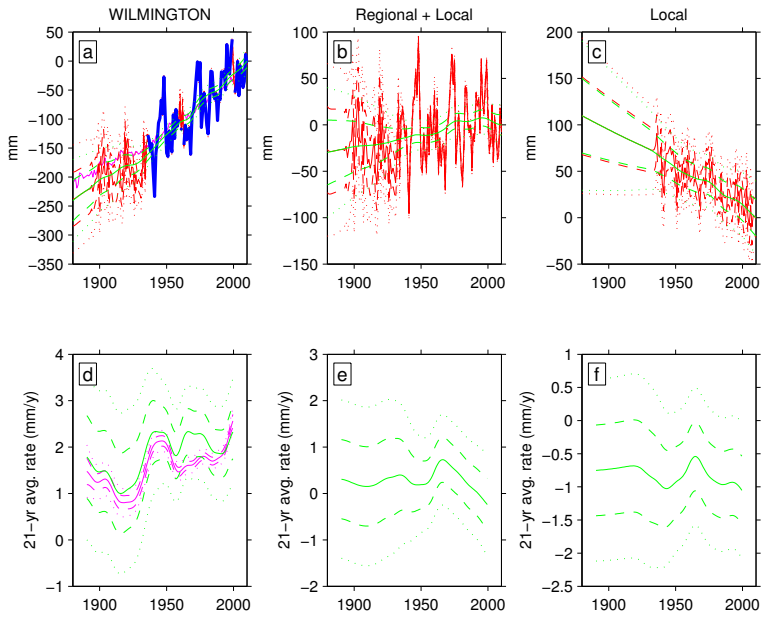

Figure S4. Sea level decomposition for the tide gauge at Wilmington.